960633

Mechanism of Soot and NOx Emission Reduction Using Multiple-Injection in a Diesel Engine

Zhiyu Han, Ali Uludogan, Gregory J. Hampson and Rolf D. Reitz
Engine Research Center
University of Wisconsin-Madison

ABSTRACT

Engine experiments have shown that with high-pressure multiple injections (two or more injection pulses per power cycle), the soot-NOx trade-off curves of a diesel engine can be shifted closer to the origin than those with the conventional single-pulse injections, reducing both soot and NOx emissions significantly. In order to understand the mechanism of emissions reduction, multidimensional computations were carried out for a heavy-duty diesel engine with multiple injections. Different injection schemes were considered, and the predicted cylinder pressure, heat release rate and soot and NOx emissions were compared with measured data. Excellent agreements between predictions and measurements were achieved after improvements in the models were made. The improvements include using a RNG k-ε turbulence model, adopting a new wall heat transfer model and introducing the nozzle discharge coefficient to account for the contraction of fuel jet at the nozzle exit. The present computations confirm that split injection allows significant soot reduction with out a NOx penalty. Based on the computations, it is found that multiple injections have a similar NOx reduction mechanism as single injections with retarded injection timings. Regarding soot reduction, it is shown that reduced soot formation is due to the fact that the soot producing rich regions at the spray tip are not replenished when the injection is terminated and then restarted. With split injections, the subsequently injected fuel burns rapidly and does not contribute significantly to soot production. The present work also demonstrates the usefulness of multidimensional modeling of diesel combustion to reveal combustion mechanisms and to provide design insights for low emission engines.

EXTENSIVE RESEARCH is in progress to reduce both nitrogen oxides (NOx) and particulate (soot) emissions from diesel engines due to environmental concerns. One of the emission-control strategies is in-cylinder reduction of pollutant production. It is well known that it is very difficult to reduce both NOx and soot production simultaneously during the combustion process. Many emission-reduction technologies developed so far tend to increase soot emission while reducing NOx emission, and vice versa. For example, retarding fuel injection timing can be effective to reduce NO formation. However, this usually results in an increase of soot production. On the other hand, although increasing fuel injection pressure can decrease soot emissions, it can also cause higher NOx emissions at the same time [1]*. Recently, it has been shown experimentally that with high-pressure multiple injections, the soot-NOx trade-off curves of a diesel engine can be shifted closer to the origin than those with single-pulse injections, reducing both soot and NOx emissions significantly [2-4].

Nehmer and Reitz experimentally investigated the effect of double-pulse split injection on soot and NOx emissions using a single-cylinder Caterpillar heavy-duty diesel engine [2]. They varied the amount of fuel injected in the first injection pulse from 10 percent to 75 percent of the total amount of fuel and found that split injection affected the soot-NOx trade-off. In general, their split-injection schemes reduced NOx with only a minimal increase in soot emissions and did not extend the combustion duration.

Tow et al. [3] continued the study of Nehmer and Reitz [2] using the same engine, and included different dwells between injection pulses and triple injection schemes in their investigation. They found that at high engine load (75%), particulate could be reduced by a factor of three with no increase in NOx and only a 2.5% increase in BSFC compared to a single injection, using a double injection with a relatively long dwell between injections. They also found that triple injection could reduce NOx and soot emissions at both light and high loads. Another important conclusion of Tow et al. [3] is that the dwell between injection pulses is very important to control soot production and there exits an optimum dwell at a particular engine operating condition. The optimum dwell of a double-injection was found to be about 10 degree crank angles at 75% load and 1600 rev/min for their engine conditions.

* Numbers in brackets designate References at the end of the paper.

Pierpont et al. [4] confirmed that the amount of fuel injected in the first pulse affects the particulate (smoke) level in experiments where the NOx emission level was held constant. However, the best double injections were found to also depend on the spray nozzle included angle. For a production injector with a 125^0 included angle, which results in significant wall impingement on the piston bowl, the best double injections were found to be those with 50% to 60% of the fuel injected in the first pulse. They also found that with a combination of EGR and multiple injections, particulate and

NOx were simultaneously reduced to as low as 0.07 and 2.2 g/bhp-hr, respectively, at 75% load and 1600 rev/min.

Other multiple injection studies can be also found in the open literature [5, 6]. The published experimental works indicate that multiple-injection is an effective mean to control NO and particulate production during the diesel combustion process. In general, multiple injections allow the injection timing to be retarded to reduce NOx emission while holding the particulate at low levels. Both the amount of fuel injected in the first pulse and the dwell between pulses are important for an optimum injection scheme.

With the application of multiple injection technology, the goal of improved injection scheme design and better control of engine combustion is made difficult by the fact that design variables are added with flexible injectors. It is thus helpful to simulate the engine processes with the use of computational models, which can provide detailed temporal and spatial information of precisely parameter-controlled injection and combustion processes.

Patterson et al. [7] performed multidimensional computations of multiple injections using an improved KIVA code. They tried to reproduce the experimental results of Nehmer and Reitz [2] and achieved a fair success. However, the accuracy of their model prediction deteriorated for double-pulse injections as the amount of fuel injected in the second pulse increased. Kong, Han and Reitz [8] modified the code by including a modified RNG k-ε turbulence model and turbulence boundary conditions [9]. Predictions of combustion and emissions of single-injections were shown to be improved significantly [8]. These successes motivated the application of the code to multiple injections in the present study.

It is clear that a good model is necessary in order to predict engine combustion and emissions accurately. Accordingly, the submodels used by Kong, Han and Reitz [8] were implemented together with improved heat transfer and injection models. The models were first applied to the experimental results of the double injections of Nehmer and Reitz [2]. For better understanding of the formation of NO and soot during multiple-injection combustion processes, a set of designed single- and double-injection schemes were computed. Based on the computational results, a mechanism of emission reduction using multiple-injection is suggested.

MODEL FORMULATION

The numerical models used are based on the KIVA-II code [10] with improvements in turbulence, gas/wall heat transfer, spray, ignition, high-temperature combustion, NOx and soot submodels. The submodels for spray breakup, ignition and combustion used in this study are those discussed in the work of Kong, Han and Reitz [8]. Briefly, the spray models include a 'blob' injection atomization model, wall-impingement hydrodynamics (rebounding/sliding) and dynamically varying drop drag coefficients to account for drop distortions from sphericity. The ignition model is based on the Shell ignition model. The combustion model is a laminar-and-turbulent characteristic-time model. These models were applied to simulate single-injection combustion in several diesel engines under a wide range of operating conditions and good agreements between predictions and measurements were obtained [8].

The turbulence, gas/wall heat transfer and emissions models are discussed here. The effects of these models on combustion predictions will be addressed in the next section.

A modified RNG k-ε model [9] was used in this study. It was shown that this model could predict more realistic large-scale flame structures compared with the k-ε model used in previous work [7]. These structures influenced in-cylinder temperature predictions and the modified model was able to quantitatively improve NOx emission prediction for single-injection combustion cases [8]. The RNG k-ε model is formulated as [9]

$$\frac{\partial \rho k}{\partial t} + \nabla \bullet (\rho \boldsymbol{u} k) = -\frac{2}{3}\rho k \nabla \bullet \boldsymbol{u} + \tau : \nabla \boldsymbol{u} + \nabla \bullet (\alpha_k \mu \nabla k) - \rho\varepsilon + \dot{W}^s \tag{1}$$

$$\frac{\partial \rho \varepsilon}{\partial t} + \nabla \bullet (\rho \boldsymbol{u} \varepsilon) = -\left[\frac{2}{3}C_1 - C_3 + \frac{2}{3}C_\mu C_\eta \frac{k}{\varepsilon}\nabla \bullet \boldsymbol{u}\right]\rho\varepsilon \nabla \bullet \boldsymbol{u} + \nabla \bullet (\alpha_\varepsilon \mu \nabla \varepsilon) + \frac{\varepsilon}{k}\left[(C_1 - C_\eta)\tau : \nabla \boldsymbol{u} - C_2 \rho\varepsilon + C_s \dot{W}^s\right] \tag{2}$$

where

$$C_3 = \frac{-1 + 2C_1 - 3m(n-1) + (-1)^\delta \sqrt{6} C_\mu C_\eta \eta}{3} \tag{3}$$

$$\delta = 1; \quad if \ \nabla \bullet \boldsymbol{u} < 0$$
$$\delta = 0; \quad if \ \nabla \bullet \boldsymbol{u} > 0$$

and

$$C_\eta = \frac{\eta(1 - \eta/\eta_0)}{1 + \beta\eta^3}, \qquad \eta = S\frac{k}{\varepsilon}$$

$$S = (2S_{ij}S_{ij})^{1/2}$$

$$S_{ij} = \frac{1}{2}\left(\frac{\partial u_i}{\partial x_j} + \frac{\partial u_j}{\partial x_i}\right)$$

In Eqs. (1)-(3), k and ε are the turbulent kinetic energy and its dissipation rate. ρ, $\boldsymbol{u}$,τ and μ are density, velocity, stress tensor and effective viscosity, respectively. η is the ratio of the turbulent-to-mean-strain time scale. S is the magnitude of the mean strain. m=0.5, and n=1.4. The C_3 term accounts for the non-zero velocity dilatation which is closed based on a rapid distortion analysis [9]. Other model constants are C_s=1.5 [10], C_μ=0.0845, C_1=1.42, C_2=1.68, α_k= α_ε=1.39, η_0=4.38, and β=0.012 [11].

A recently developed temperature wall function model [12] was used to predict gas/wall convective heat transfer. This model is derived from the one-dimensional energy conservation equation and accounts for the effect of thermodynamic variations of gas density and the increase of the turbulent Prandtl number in the boundary layer. Due to the density variation of the gas, the dimensionless temperature is found to be proportional to the logarithmic ratio of the flow temperature to the wall temperature instead of to the arithmetic difference of the two temperatures, which is the case for incompressible flows [13]. The advantages of this model include the ability to use a relative coarse grid size near the wall with accurate heat transfer predictions. With the use of

this model, Han and Reitz reproduced the measured heat fluxes in a homogeneous charge engine [12]. The heat flux at the wall is calculated as

$$q_w = \frac{\rho c_p u^* T \ln(T/T_w)}{2.1\ln(y^+) + 2.513} \quad (4)$$

where

$$y^+ = \frac{u^* y}{\nu} \quad (5)$$

$$u^* = \left(C_\mu^{1/2} k\right)^{1/2} \quad (6)$$

In Eqs. (4) to (6), q_w is the heat flux through the wall; c_p is heat capacity; T is the gas temperature; T_w is the wall temperature; y is the distance from the wall and ν is molecular viscosity. Noticed that the effects of source terms (such as chemical heat release and unsteadiness) are not included in Eq. (4) since they were shown to be insignificant [12].

The 'blob' injection model of Reitz [14] is used in the present study. It is assumed in this model that the injected drop parcels have the same sizes as the nozzle exit diameter. The advantage of this assumption is that uncertainties related to the effects of the internal nozzle-passage flow and nozzle geometry on initial disturbances and the atomization process can be incorporated into just one model constant. However, this makes it difficult to model injectors with different nozzle geometry. Recent experiments have confirmed that processes such as supercavitation take place at the nozzle exit under normal diesel injection conditions and the measured flow velocity is close to the velocity calculated from the pressure drop assuming inviscid incompressible flow [15]. This indicates that an effective nozzle section area and a corresponding effective flow diameter should be used in the computation instead of the geometric nozzle exit area and diameter. In this way, the contraction of fuel jet can be included in the atomization model. Therefore, spray characteristics affected by different nozzle contraction effects (i.e., different discharge coefficients), which influence combustion characteristics and emissions, could be modeled. Based on the above argument, the discharge coefficient of an injector nozzle, C_D, is used in the spray atomization model in this study. That is

$$A_e = C_D A_0 \quad (7)$$

or

$$r = \sqrt{C_D}\, r_o \quad (8)$$

and, to satisfy fuel mass flow conservation

$$V_e = V_0 / C_D \quad (9)$$

where A_e and V_e are the effective nozzle cross-section area and fuel jet exiting velocity used in the model, respectively; A_0 and r_o are the geometric section area and radius of the nozzle, respectively; r is the effective nozzle radius corresponding to A_e, and V_0 is the jet exiting velocity corresponding to A_0. Again, r and V_e are used as the initial parameters in the atomization model in the present study. The effect of C_D will be discussed later.

The current approach to modeling NO production is with the Extended Zel'dovich mechanism [7]. When comparing with experimental NOx data, a constant factor of 1.533 (the ratio of the molecular masses of NO_2 to NO) is applied to the NO predictions. The Extended Zel'dovich Mechanism consists of the following equations as described by Bowman [16]

$$O + N_2 \text{ <--> } NO + N \quad (10)$$

$$N + O_2 \text{ <--> } NO + O \quad (11)$$

$$N + OH \text{ <--> } NO + H \quad (12)$$

With the partial equilibrium of Eq. (13) for the hydrogen radicals,

$$O + OH \text{ <--> } O_2 + H \quad (13)$$

and a steady state assumption for N, which results from setting d[N]/dt=0 in the rate equations resulting from Eqs. (10), (11), and (12), the Extended Zel'dovich mechanism can be written as a single rate equation for NO, as originally put forth by Heywood [17],

$$\frac{d}{dt}[NO] = 2k_{1f}[O][N_2]\left\{\frac{1-[NO]^2/K_{12}[O_2][N_2]}{1+k_{1b}[NO]/\left(k_{2f}[O_2]+k_{3f}[OH]\right)}\right\} \quad (14)$$

where $K_{12}=(k_{1f}/k_{1b})(k_{2f}/k_{2b})$ and the subscripts 1, 2 and 3 refer to Eqs. (10), (11) and (12), respectively. O, OH, O_2 and N_2 are assumed to be in local thermodynamic equilibrium. The rate constants as recommended by Bowman [16] are:

$$k_{1f} = 7.6\text{x}10^{13} \exp(-38{,}000/T)$$
$$k_{1b} = 1.6\text{x}10^{13} \quad (15)$$

$$k_{2f} = 6.4\text{x}10^{9}\, T \exp(-3150/T)$$
$$k_{2b} = 1.5\text{x}10^{9}\, T \exp(-19{,}500/T) \quad (16)$$

$$k_{3f} = 1.0\text{x}10^{14}$$
$$k_{3b} = 2.0\text{x}10^{14} \exp(-23{,}650/T) \quad (17)$$

Since a number of other NOx mechanisms are believed also to be important in spray and diffusion flames, work is in progress to explore these other mechanisms, such as non-equilibrium radials, N_2O intermediate, prompt NO, NO_2, and turbulent mixing effects [18].

Hiroyasu [19] developed a simple soot model which was later applied to multidimensional diesel combustion by Belardini et al. [20]. The model predicts the production of soot mass, M_s, by a single-step competition between the soot mass formation rate, $\dot{M}_{sf}$, and the soot mass oxidation rate, $\dot{M}_{so}$, according to

$$\frac{d(M_s)}{dt} = \dot{M}_{sf} - \dot{M}_{so} \quad (18)$$

The Arrhenius formation rate is proportional to the fuel vapor mass, M_{fv}, as given by

$$\dot{M}_{sf} = K_f M_{fv} \quad (19)$$

where the formation coefficient is a function of pressure (bar) and temperature (K) according to

$$K_f = A_{sf} P^{0.5} exp(-E_{sf} / RT) \quad (20)$$

The Arrhenius oxidation rate is proportional to the soot mass,

$$\dot{M}_{so} = K_o M_s \quad (21)$$

and the oxidation coefficient is a function of pressure, temperature and the oxygen mole fraction, X_{O2},

$$K_o = A_{so} X_{O2} P^{1.8} exp(-E_{so} / RT) \quad (22)$$

The single-step, two process Hiroyasu soot model is shown schematically below as fuel mass going to soot mass and soot mass going to oxidation products (e.g. CO)

Fuel ---- Kf -----> Soot --- K_o ---> CO (23)

The Hiroyasu soot model has been modified in the present study by replacing the Arrhenius global oxidation rate equation with the experimentally based oxidation rate of Nagle and Strickland-Constable (NSC) [21]. Based on the oxidation experiments of carbon graphite in an O_2 environment over a range of partial pressures, the oxidation rate is modeled by two mechanisms whose rates depend on the surface chemistry involving more reactive "*A*" sites and less reactive "*B*" sites and the conversion of "*A*" sites to "*B*" sites. With the above formulation of the soot mass oxidation rate, the oxidation rate coefficient of Eq. (22) is replaced by the NSC oxidation rate coefficient

$$K_o = \frac{6}{\rho_s D_{nom}} \dot{W}''_{nsc} \quad (20)$$

where $\dot{W}''_{nsc}$ is the NSC soot mass oxidation rate per unit surface area (gram-carbon/sec-cm^2), D_{nom} is a nominal spherical soot particle size, taken to be 25 nm, the soot density ρ_S is taken to be 2.5 g/cm^3. More details of the NSC oxidation model are given by Hampson and Reitz [22].

COMBUSTION MODELING OF MULTIPLE-INJECTION

Engine and Measurements

The KIVA-II model predictions were compared with experimental data from a single-cylinder version of the Caterpillar 3406 heavy-duty truck engine. The emissions data, given in Table 1, were measured by Nehmer and Reitz [2]. The engine specifications used in the experiments and computations are listed in Table 2. The injector used in the experiments was a common-rail system with six holes and 0.259 mm hole diameters. The injection pressure was 90 MPa.

The labeling scheme in Table 1 for the split injection case gives the percent of the fuel injected in the first and last pulses, and the dwell between two injections. For instance, 75-8-25 represents 75 percent fuel injected in the first pulse, 25 percent in the second, and an eight crank angle degree dwell between the two injection pulses. The value of NOx [2] were adjusted to be based on mass NO_2 as mentioned before.

The computations used tetradecane ($C_{14}H_{30}$) as the fuel due to its similar C/H ratio to the used diesel fuel (the fuel used in the experiments was Amoco Premier #2). The computational mesh used represents one-sixth of the engine combustion chamber (i.e., a 60-degree sector) for computational efficiency, since the injector has six injector holes. There were 20 cells in the radial direction, 30 cells in the azimuthal direction and 18 cells in the axial direction with 5 cells in the squish region at top dead center. This mesh resolution, seen in Fig. 1, has been found to give adequately grid-independent results by Han and Reitz [9].

Table 1 Measured Emissions data for single and multiple injections.

Case No.	Eqv. Ratio	Inj. Timing (BTDC) (Nominal)	Soot (g/bhp-hr)	NOx (g/bhp-hr)
Baseline	0.461	13	0.083	5.72
10-3-90	0.501	12	0.163	4.26
10-8-90	0.494	16	0.184	4.02
25-3-75	0.451	14	0.095	4.66
25-8-75	0.453	15	0.084	4.88
50-3-50	0.455	12	0.100	5.40
50-8-50	0.454	13	0.083	5.15
75-3-75	0.473	12	0.076	6.02
75-8-25	0.455	12	0.074	5.81

Table 2 Engine specifications and conditions.

Cylinder bore x stroke (mm)	137.6 x 165.1
Connecting rod length (mm)	261.62
Displacement volume (L)	2.44
Compression ratio	15.1
Number of nozzle orifice x diameter (mm)	6 x 0.259
Spray angle (from cylinder head) (degrees)	27.5
Combustion chamber	Quiescent
Piston crown	Mexican hat
Inlet air pressure (kPa)	184
Inlet air temperature (K)	310
Intake valve closure (deg. BTDC)	−147
Swirl ratio (nominal)	1.0
Engine speed (rev/min)	1600
Fuel	Amoco Premier #2
Injection system	Common Rail
Injection pressure (MPa)	90

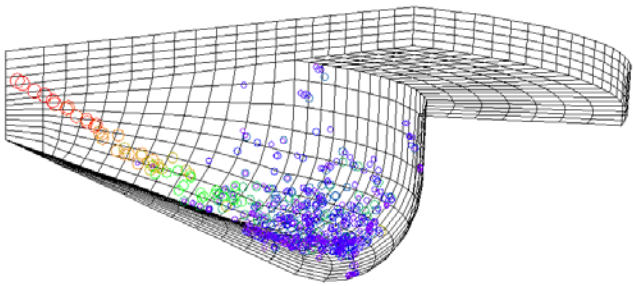

Figure 1 Outline of the computational mesh at TDC. Spray droplets (circles) are superimposed for reference.

The Effects of Model Formulation

The effects of the various model formulations have been studied. As discussed before, the present code uses the modified RNG k-ε model (Eqs. (1)-(2)), the compressible-flow heat transfer model (Eq. (4)) and the discharge coefficient of the nozzle (Eqs. (7)-(9)). Previous work [7] used the standard k-ε model and the KIVA heat transfer model [10]. The predicted cylinder pressures and heat release rates by using the present and the previous model are shown in Fig. 2 for the 50-8-50 split-injection case listed in Table 1. The zero-d (also called 'measured') heat release rate results are calculated by using an in-house zero-dimensional code and the measured pressure data. As can be seen the agreement between prediction and measurement is improved significantly by using the present model. Particularly, the previous model [7] underpredicts the third peak of the heat release rate curve greatly which indicates that the diffusion combustion that results from the second-pulse injection is not modeled accurately.

Computations were carried out to assess the extent to which the individual models contribute to the differences seen in Fig. 2. The approach used here was to change one model at

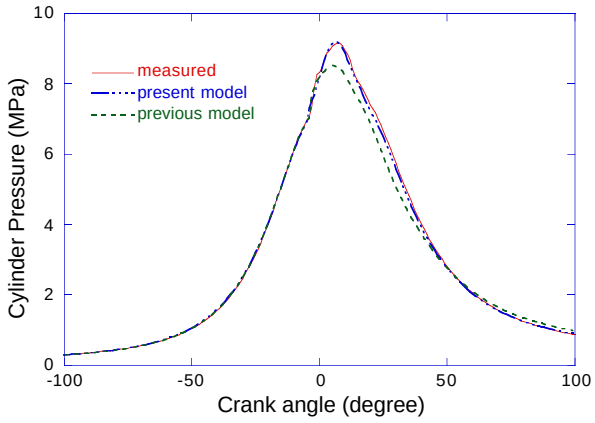

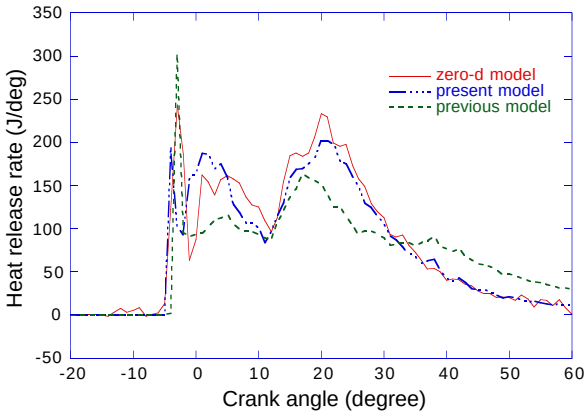

Figure 2 Comparison showing improvements in multiple-injection combustion predictions using the present model.

a time and to keep the others the same. The effect of the turbulence model is shown in Fig. 3. When the standard k-ε model is used, the combustion prediction deteriorates, which is evidenced by the underprediction of the fuel burning rate of the second injection pulse that is seen in the heat release rate curves. Due to the slower combustion of the second injection pulse predicted by using the standard k-ε, combustion extends later into the expansion stroke, therefore, the predicted cylinder pressure is higher than the measured one during the later expansion stroke.

Two gas/wall heat transfer models, namely, the present model and the KIVA model [10], were tested. Figure 4 shows the predicted wall heat fluxes using the two models. The monitoring location is over the piston bowl at the edge of the bowl on the cylinder-head surface. As can be seen, the present model predicts as high as 5.6 MW/m^2 peak heat flux during combustion, which is in the range of previous measured values in heavy-duty diesel engines [17]. The KIVA heat transfer model is based on Reynolds analogy [10] and does not account for gas compressibility. This model was shown to significantly underpredict heat flux in a gasoline engine by Reitz [23]. In the case discussed in Fig. 4, the heat flux predicted by using this model is also very low. It is known that in conventional engines heat is transferred into the cylinder (heating the gas) also in the earlier portion of the compression stroke, since the gas temperature is lower than the wall temperature at this time [17]. This heat transfer

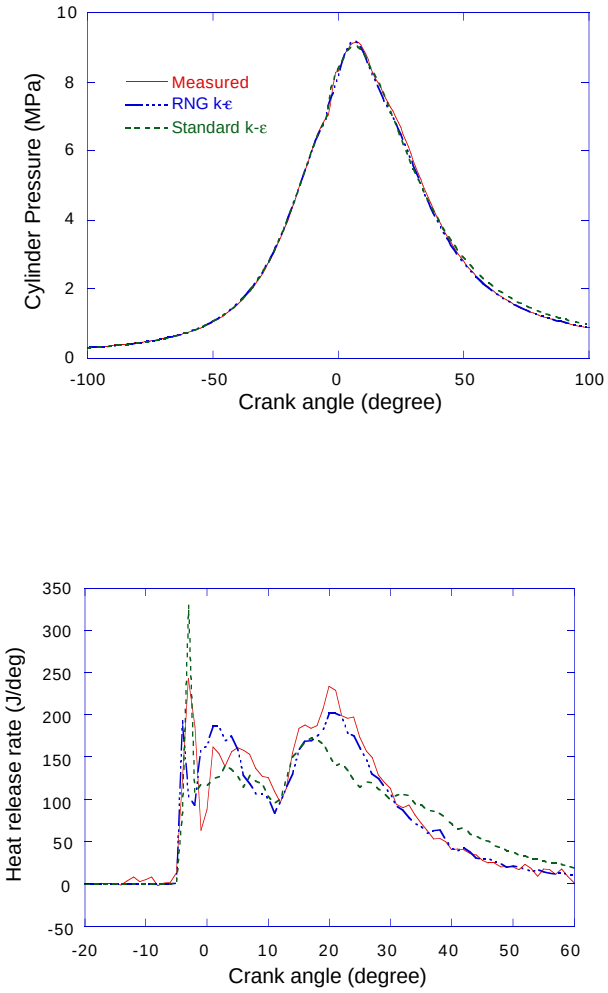

Figure 3 Effect of turbulence model on combustion prediction.

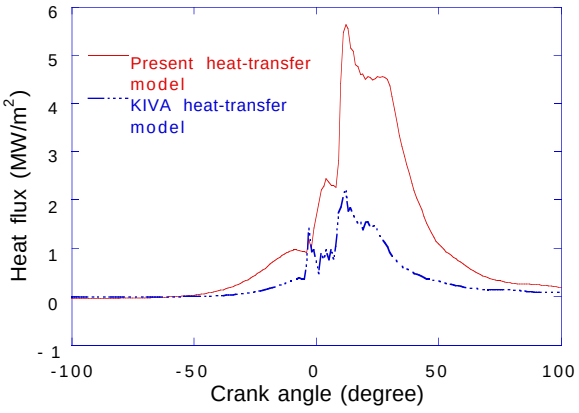

Figure 4 Predicted wall heat fluxes. The monitoring location is over the piston bowl at the edge of the bowl at the cylinder-head surface in the plane of the spray.

characteristic is also predicted by the present model. As can be discerned in Fig. 4, the present model predicts negative heat flux (heat is transferred into the cylinder) in the early compression stroke and positive heat flux (heat is transferred out of the cylinder) after about 50 degrees before top dead center, while the standard KIVA model predicts a positive heat flux throughout the cycle, which is physically incorrect.

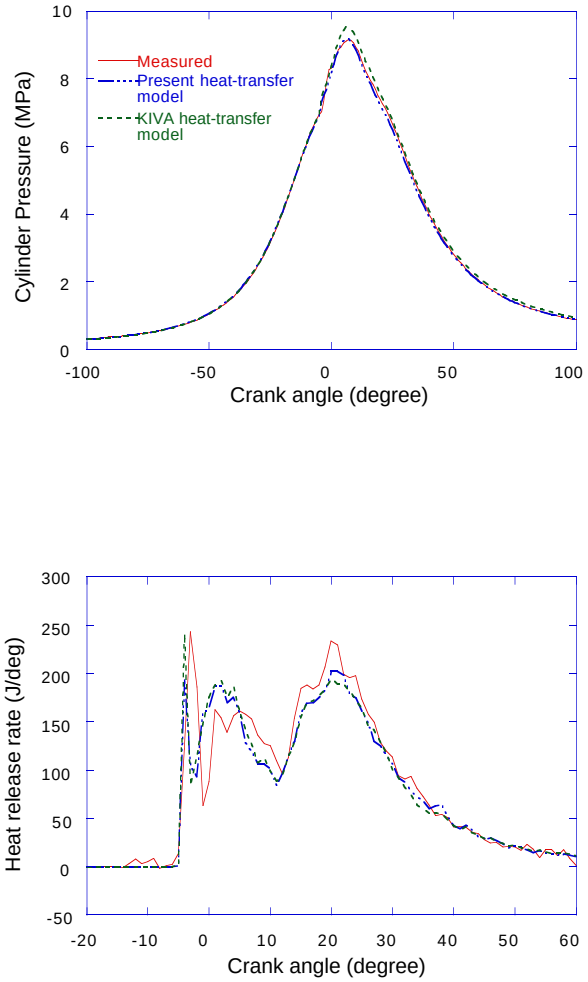

Figure 5 Effect of gas/wall heat transfer model on combustion prediction.

The effect of the heat transfer prediction on combustion modeling is illustrated in Fig. 5. Since the standard KIVA heat transfer model underpredicts heat loss, the cylinder pressure (which indicates the engine work output) is overpredicted due to energy conservation. On the other hand, the two heat transfer models do not result in a significant difference in the heat release rate except that the premixed-burn peak is somewhat higher using the standard KIVA model. In

the present multidimensional code, heat release is calculated from the chemical energy released during combustion, therefore, heat loss through the wall does not directly affect the combustion calculation. However, it does affect the evolution of combustion by affecting the gas thermal field.

As discussed before, the discharge coefficient of injector nozzle, C_D, is introduced in the present computations. In the engine considered, a common rail injector is used and the nozzle discharge coefficient is set to be 0.7 based on the measured data of Tow [24]. Its effect on the combustion prediction is shown in Fig. 6. With the use of C_D=0.7, the spray velocity increases (see Eq. (9)) which increases the momentum of the spray. As a result, drop breakup is increased, fuel-air mixing is enhanced, and better prediction of combustion is achieved.

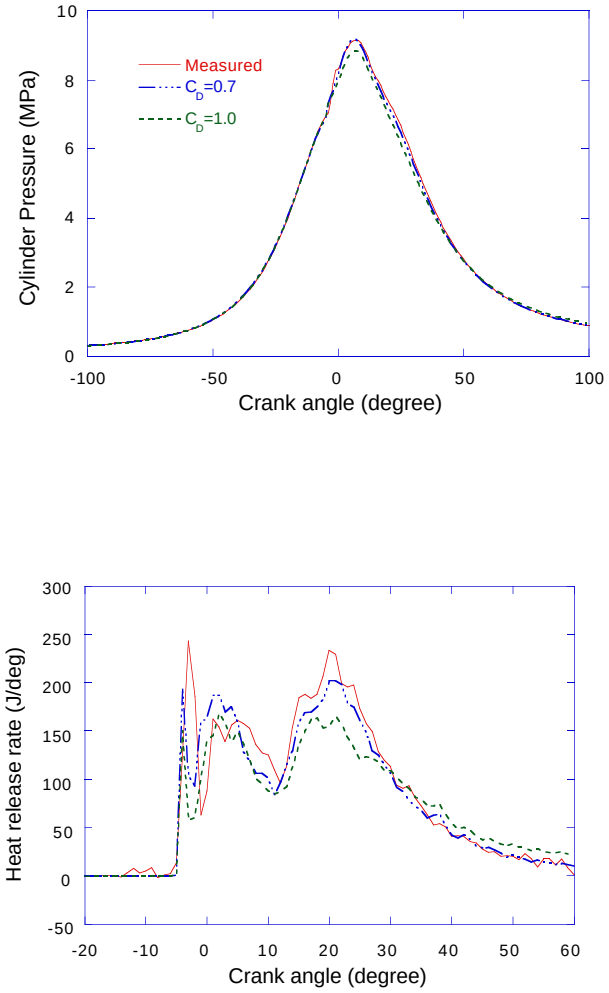

Figure 6 Effect of nozzle discharge coefficient on combustion prediction.

Predictions and Comparison with Measurements

First, single injection cases were predicted to verify the accuracy of the model predictions. The baseline case with injection timing of 10.5 degrees BTDC was chosen due to its similar injection timing to that used for the split injection cases. The heat release rate and the pressure predictions are compared in Fig. 7 with measured data. The predicted pressure and heat release rate shows a reasonably good agreement. The over-prediction of the heat release rate after the premixed-burn period could indicate that the initial flame spread rate is overestimated, as also discussed by Ricart and Reitz [25].

The eight different injection schemes indicated in Table 1 were simulated next. Figures 8 and 9 show the pressure and heat release rate for all 8 split injection cases, with 3 and 8 crank degree dwells between injections, respectively. The results show a very good agreement between the predictions and the measurements except that the premixed-burn is underpredicted somewhat in the schemes where 10% fuel is injected during the first injection pulse. Accurate prediction of the heat release rate and pressure is required in order to be able to predict the soot and NOx emissions [7].

Soot and NOx predictions were also performed for the baseline single injection and the split injection cases. The results are given in Table 3. No model constants were changed during the computations. As can be seen in Table 3, the

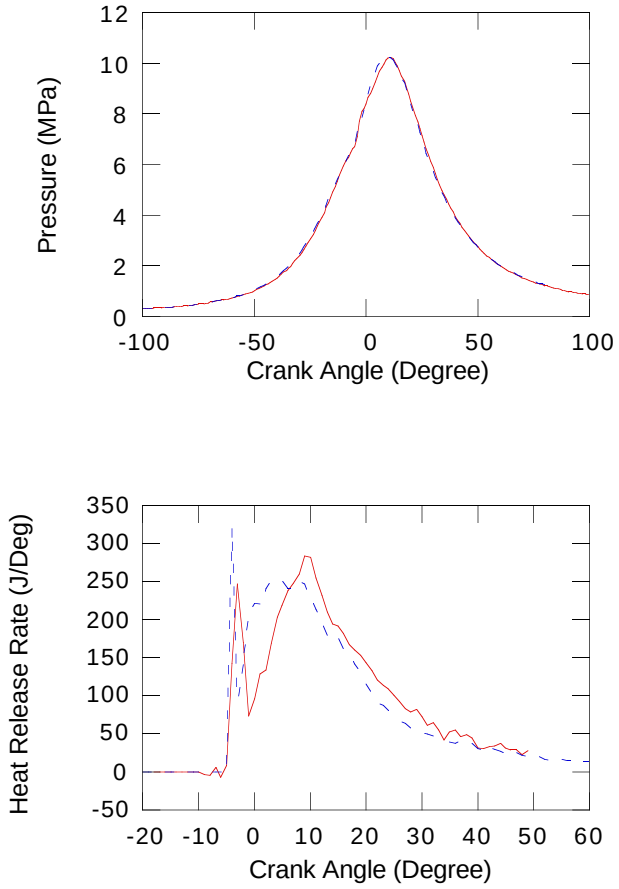

Figure 7 Single injection predictions. Spray injection timing is 10.5 degrees BTDC. Solid line--measured, dash line--predicted.

Table 3 Comparison the predicted and measured NOx and soot emissions.

Case No.	Measured particulate (g/bhp-hr)	Calculated Soot (g/bhp-hr)	Measured NOx (g/bhp-hr)	Calculated NOx (g/bhp-hr)

Baselin	0.083	0.078 e	5.72	6.28
10-3-90	0.163	0.200	4.26	3.78
10-8-90	0.184	0.190	4.02	4.11
25-3-75	0.095	0.08	4.66	4.18
25-8-75	0.084	0.067	4.88	4.04
50-3-50	0.100	0.16	5.40	5.16
50-8-50	0.083	0.07	5.15	4.45
75-3-25	0.076	0.078	6.02	5.61
75-8-25	0.074	0.069	5.81	5.10

predictions agree reasonably well with the measured values. In general, the NOx predictions agree with the measured data to within 15%, while the soot is predicted to within 20% of the measured particulate in most cases. The 10-3-90 and 50-3-50 cases over predict the soot by larger amounts. However, it is fair to say that generally there is a good agreement with the measured values and trends.

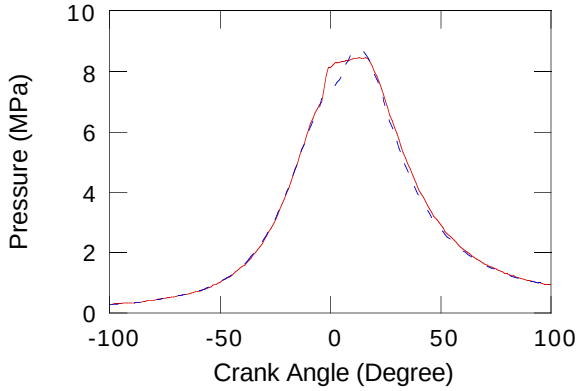

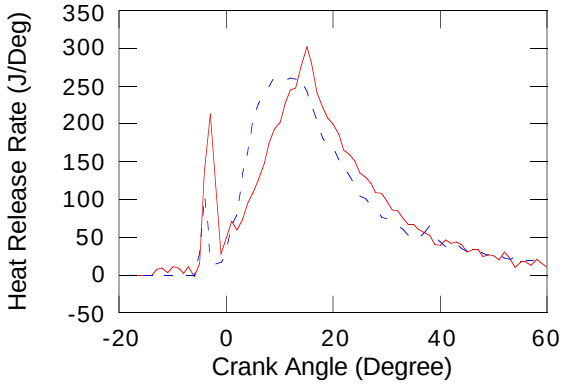

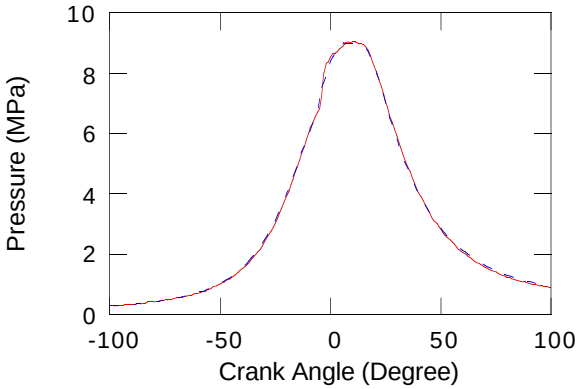
Pressure (MPa)
10
8
6
4
2
0
-100
-50
0
50
100
Crank Angle (Degree)

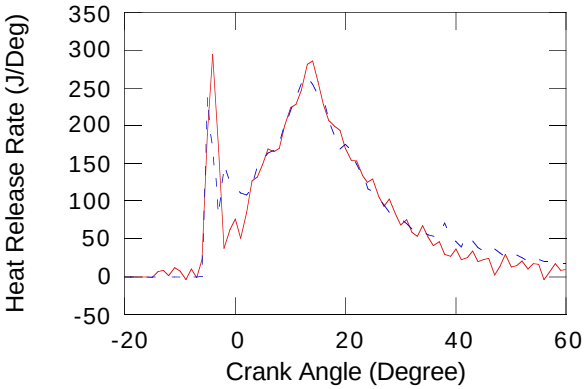
Heat Release Rate (J/Deg)
350
300
250
200
150
100
50
0
-50
-20
0
20
40
60
Crank Angle (Degree)

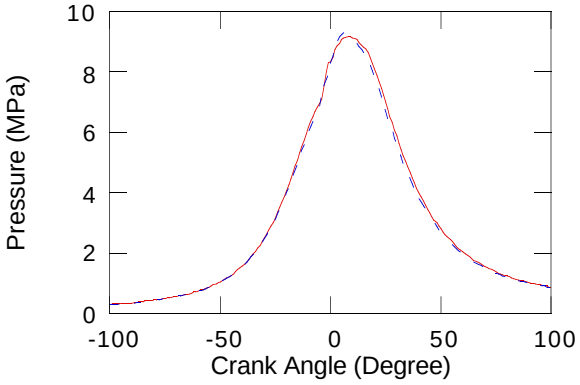
Pressure (MPa)
10
8
6
4
2
0
-100
-50
0
50
100
Crank Angle (Degree)

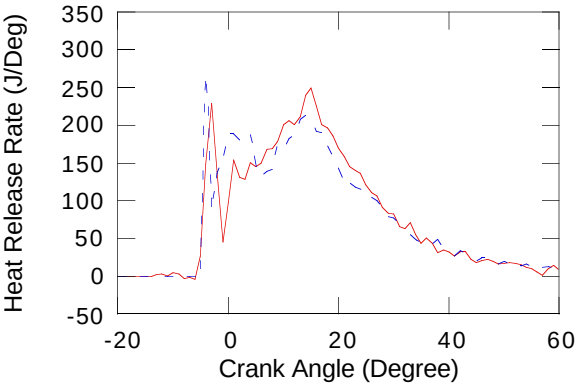
Heat Release Rate (J/Deg)
350
300
250
200
150
100
50
0
-50
-20
0
20
40
60
Crank Angle (Degree)

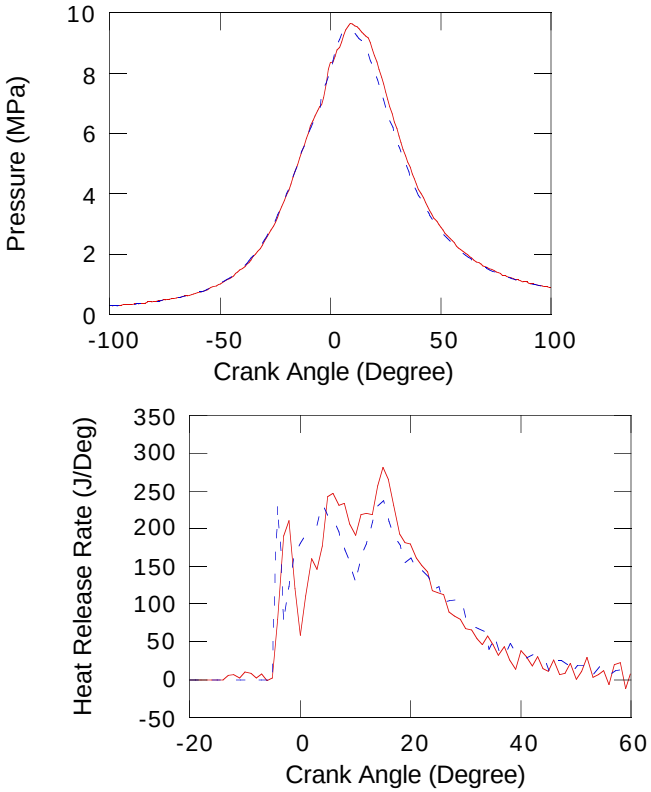

Figure 8 Pressure and heat release rate predictions for split injections. The dwell between the two injection pulses is three degrees. Solid line--measured, dash line--predicted. From top: 10-3-90, 25-3-75, 50-3-50 and 75-3-25.

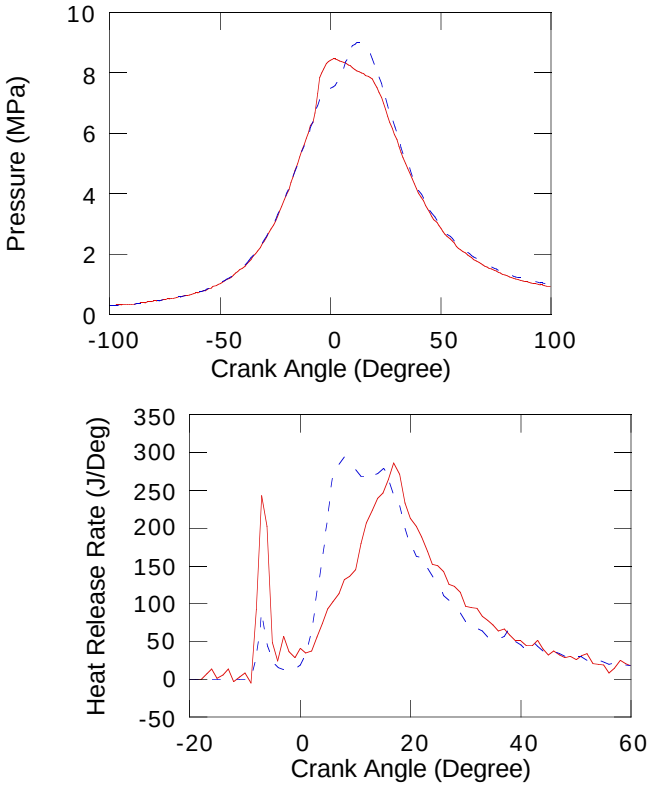

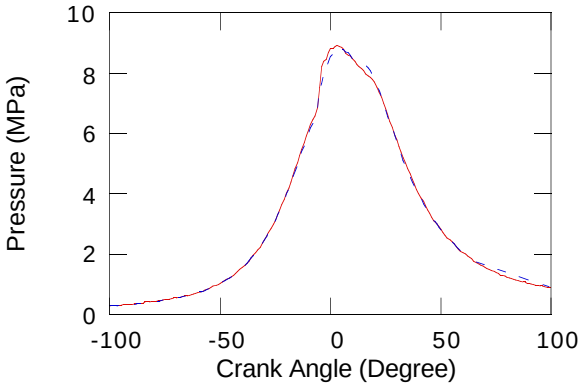
Pressure (MPa)
10
8
6
4
2
0
-100
-50
0
50
100
Crank Angle (Degree)

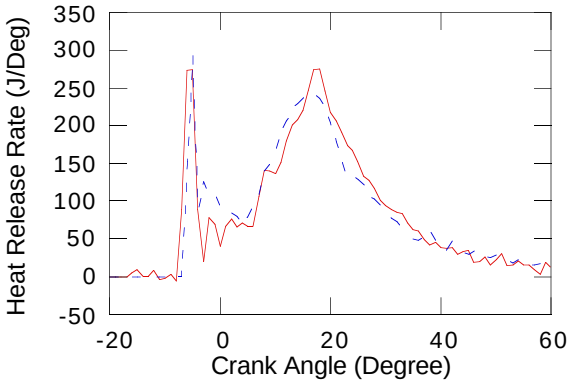
Heat Release Rate (J/Deg)
350
300
250
200
150
100
50
0
-50
-20
0
20
40
60
Crank Angle (Degree)

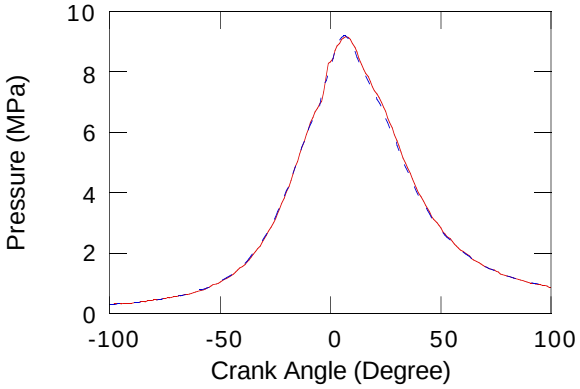
Pressure (MPa)
10
8
6
4
2
0
-100
-50
0
50
100
Crank Angle (Degree)

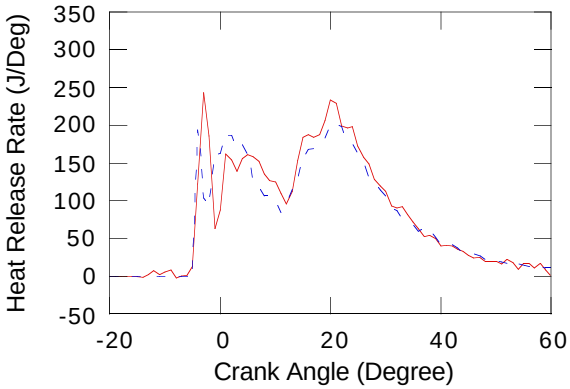
Heat Release Rate (J/Deg)
350
300
250
200
150
100
50
0
-50
-20
0
20
40
60
Crank Angle (Degree)

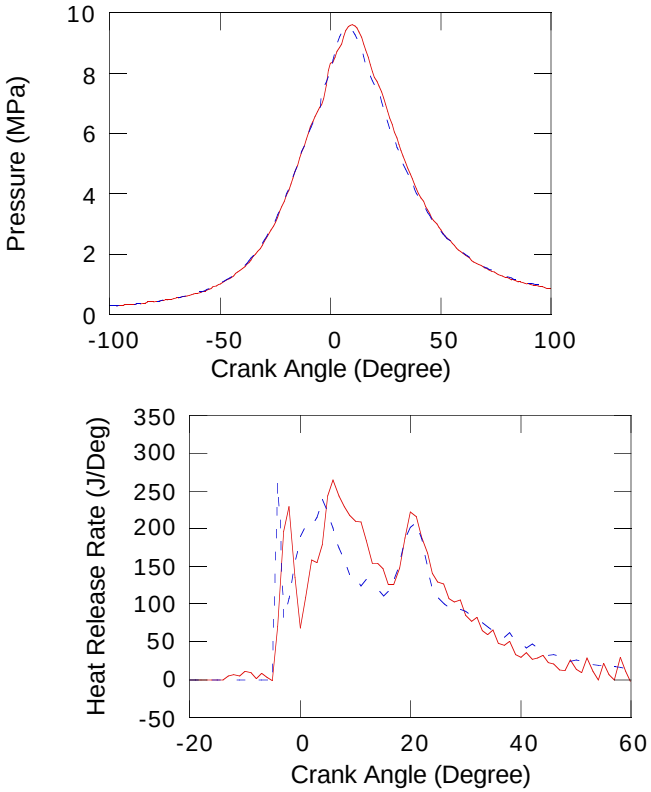

Figure 9 Pressure and heat release rate predictions for split injections. The dwell between the two injection pulses is eight degrees. Solid line--measured, dash line--predicted. From top: 10-8-90, 25-8-75, 50-8-50 and 75-8-25.

MECHANISM OF EMISSIONS REDUCTION

The above comparisons of computation and measurement give confidence in the combustion and emission prediction capabilities of the present model. In order to further study the mechanism of emissions reduction using multiple injections, a set of injection schemes was designed and computed which included three single injections and three double injections. The injection schemes are shown schematically in Fig. 10. In the nomenclature 75-8-25 (-10), the number in the brackets indicates the injection starting angle (ATDC). The same amount of fuel is injected in all the cases considered. The needle lift is simply modeled by using one (or two) step functions with the same step height to keep the same injection velocity in all cases. In all the double injections, the total injection duration is 28 degrees, and in the first two single injections, the injection duration is 20 degrees. In the last case, the injection duration is 8 degrees longer than the other single injection cases, and hence the nozzle radius was reduced by 15.5% to keep the same amount of fuel injected. Figure 11 indicates the injected fuel history for each case. With the use of the designed schemes, the possible effects of differences in equivalence ratio and injection timing in the experimental cases (see Table 1) are eliminated. Besides, the designed schemes are not far from the experimental ones, hence the computed results can be confidently used, based on the good agreement with the experiments discussed before.

The predicted combustion is illustrated in Fig. 12 which shows the burnt fuel as a function of crank angle. It is seen that the fuel-burnt history curves of the double injections are embraced by those of the two single injections with the 20-degree injection duration. The double-injections follow the single (-10) case during the time corresponding to the first injection-pulse and then become close to the single (-2) case during the time corresponding to the second injection-pulse. Between the injection pulses, a transition occurs due to the dwell period of the injection. The time at which the transition starts depends on the amount of fuel injected in the first injection-pulse. These features indicate that the double-injection combustion is partly the same as, or close to, either of the single-injections from a macroscopic viewpoint. However, the combustion process is complicated by the second injection-pulse after the dwell between injections. For example, combustion in the 25-8-75 (-10) case differs from that in the single (-10) case soon after ignition, which is due to the non-linear effects of fuel vaporization and mixing. The fuel-burnt curve of the single (-10, duration 28) case which has a 28-degree injection duration is also included within those of the two single-injections with 20-degree injection duration. However, as can be seen, it does not follow or become close to any portion of them after ignition.

The computed soot-NOx trade-off is shown in Fig. 13 for the various cases. It is again confirmed that double injections are effective at reducing soot and NOx emissions. For example, the soot emission of the single (-10) case is reduced by a factor of 4 using the 75-8-25 (-10) injection while the NO emission is increased very slightly, as indicated in Fig. 13. When the 50-8-50 (-10) double injection is used, both the soot and NO emissions are reduced below those of the single (-10) case. However, when the 25-8-75 (-10) double injection is

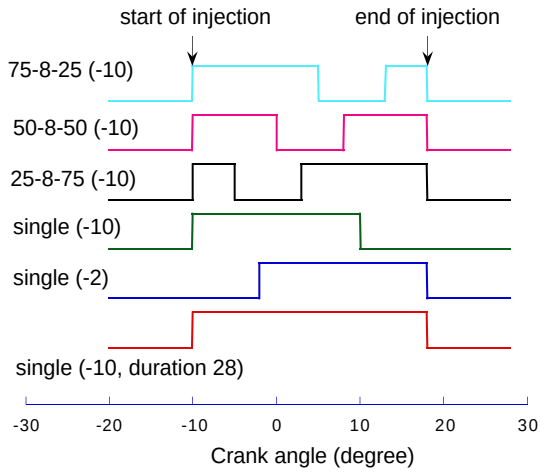

Figure 10 Schematic showing model injection schemes.

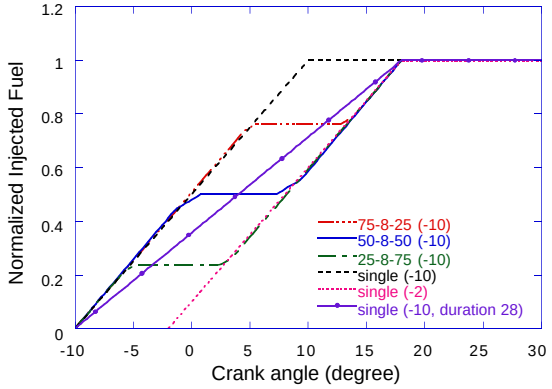

Figure 11 Injected fuel as function of crank angle. The injected fuel is normalized by the total injected fuel.

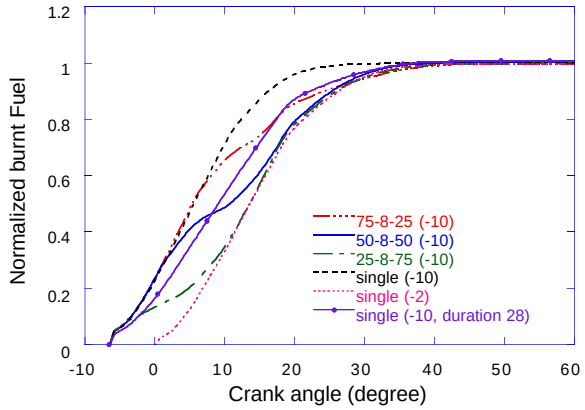

Figure 12 Fuel burnt histories showing combustion evolution. The burnt fuel is normalized by the total injected fuel.

used, the soot emission is increased significantly at the same time that the NO emission is reduced greatly.

It is of interest to examine the reasons for these observed emissions reductions. In general, the NO emissions are reduced by using the double injections studied here and the soot emissions are reduced in some cases. It is noticed that soot and NO are also reduced relative to the single (-10, duration 20) case with the use of the single (-10, duration 28) scheme. Since combustion of this case is similar to that of the 50-8-50 (-10) double injection as indicated in Fig. 12, this case results in about the same level of soot and NO emissions, as seen in Fig. 13. However, this scheme would require the use of smaller nozzle hole sizes in applications.

NO REDUCTION MECHANISM - The predicted accumulated in-cylinder NO-formation history vs. burnt fuel mass is shown in Fig. 14. As can be seen, the NO formation history of the 75-8-25 (-10) case is very similar to that of the single (-10) case. The injection pause does not affect NO formation significantly and combustion of the 25% fuel in the second injection pulse only causes a small increase in NO production. However, the effect of the injection pause becomes more significant in the 25-8-75 (-10) case. It delays the major portion of the combustion and reduces the NO formation rate considerably compared with the single (-10) case. Comparing the 25-8-75 (-10) case with the single (-2) case in which the injection timing is retarded 8 degrees, their NO formation rates become similar during the major portion of the combustion, as also seen in Fig. 14. These phenomena are closely related to the combustion evolution histories in Fig. 15 in which the heat release rates are given. Although combustion in the 25-8-75 (-10) and single (-2) cases are quite different before 10 degrees ATDC due to their different injection timings, combustion of the fuel in the second pulse is delayed by the injection pause in the former case. As a result, the major portion of combustion in the 25-8-75 (-10) case becomes similar to that of the single (-2) case after 10 degrees ATDC.

It is also noticed in Fig. 15 that combustion in the 75-8-25 (-10) case becomes very different from that of the single (-10) case after 5 degrees ATDC since this is the time that the injection is paused. However, the NO formation histories of the two cases are not very different as discussed before in Fig. 14. It is known that NO formation is very sensitive to the gas temperature during combustion. As can be seen in Fig. 16, which gives the mixture mass fraction with temperatures greater than 2200 K vs. fuel mass burnt, the evolution of the high-temperature gas mixture in the 25-8-75 (-10) case is similar to that of the single (-2) case after 25% of the fuel is burnt. The greater amount of high-temperature gas before 25% fuel is burnt in the former case results in the slightly higher NO level seen in Fig. 14. It is also seen that the 75-8-25 (-10) and single (-10) cases have almost the same high-temperature gas histories before 80% of the fuel is burnt. Hence, they have very similar NO formations. By comparing Fig. 14 with Fig. 16, it is of interest to notice that the large gas temperature difference between the 75-8-25 (-10) and single (-10) cases seen in the later stage of combustion does not affect the NO formation significantly, while the relatively smaller temperature differences between the 25-8-75 (-10) and single (-2) cases in the earlier stage of combustion result in relatively larger changes in the NO formations. This can be explained by the fact that the NO chemistry is sensitive to the early combustion details because these combustion products stay at a high temperature for the longest time, and the combustion

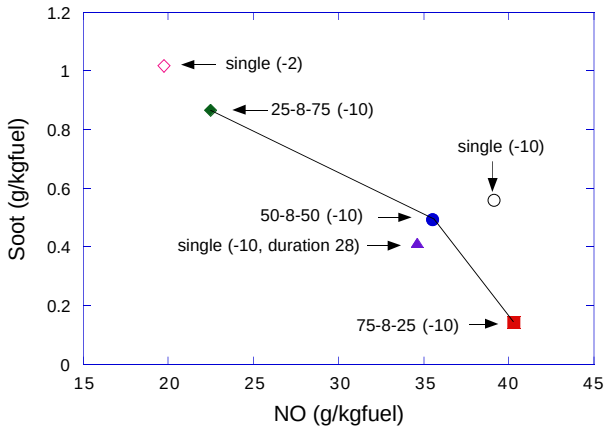

Figure 13 Computed soot-NO trade-off of the designed injection schemes.

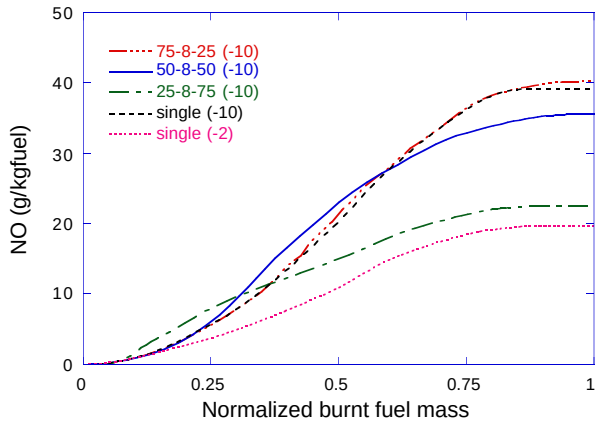

Figure 14 NO formation history as the function of burnt fuel mass. The burnt fuel is normalized by the total injected fuel. The single injection cases have a 20-degree duration.

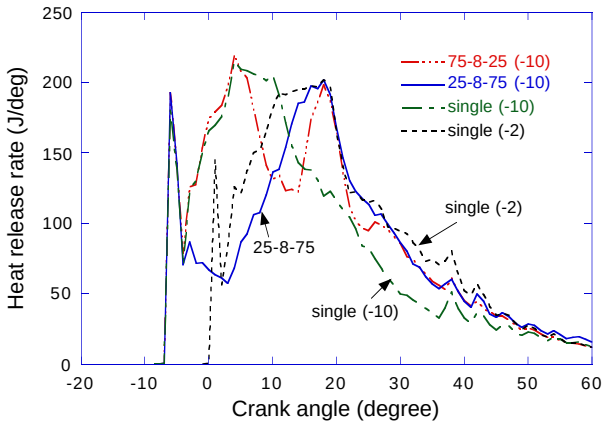

Figure 15 Computed heat release rates for the single and double injection schemes.

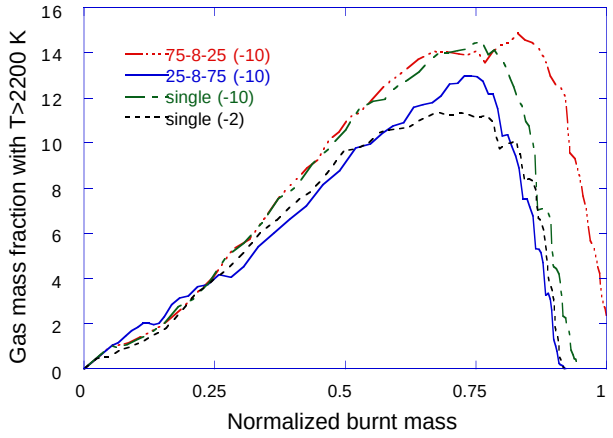

Figure 16 In-cylinder high-temperature mixture fractions. The burnt fuel is normalized by the total injected fuel.

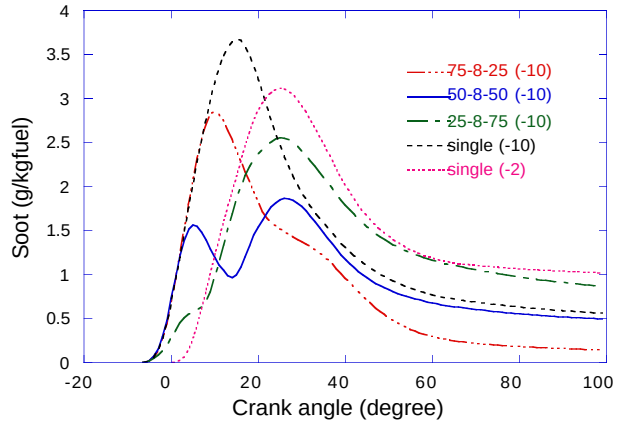

Figure 17 In-cylinder soot production history for single and double injection schemes.

region is not cooled by the vaporization of the continuously injected fuel that occurs in the single injection case. The NO chemistry is effectively frozen after about 80% of the fuel is burnt in all the cases considered (see Fig. 14) because the late-burning mixture has a shorter residence time at a high temperature due to the piston expansion.

Based on the above discussion, the NO reduction mechanism of multiple injections is similar to that of retarding the injection timing. With the use of multiple injections, combustion of the second-pulse injected fuel is delayed by the injection pause. When the percentage of the first-pulse injected fuel is large (75% in Fig. 14), the NO formation history of the double injection is like that at a single injection with the same injection timing. The effect of combustion of the second-pulse injected fuel does not influence the NO formation significantly. As the percentage of the fuel in the first injection pulse becomes small (e.g., 25%), the NO formation rate of the double injection becomes similar to that of a single injection retarded with the dwell-time of the double injection. In this case, combustion of the first-pulse injected fuel has an important effect on NO production, and it results in more NO being formed in the earlier combustion stage, and hence more total NO production.

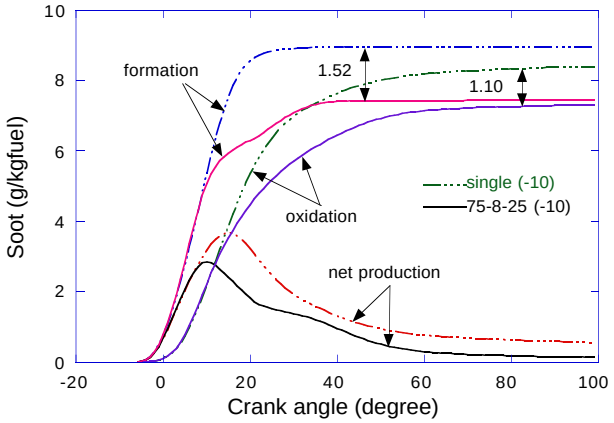

Figure 18 In-cylinder histories of soot formation, oxidation and net production.

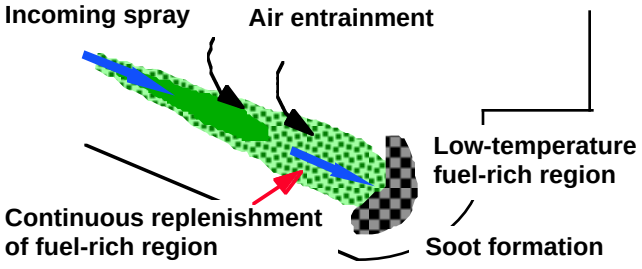

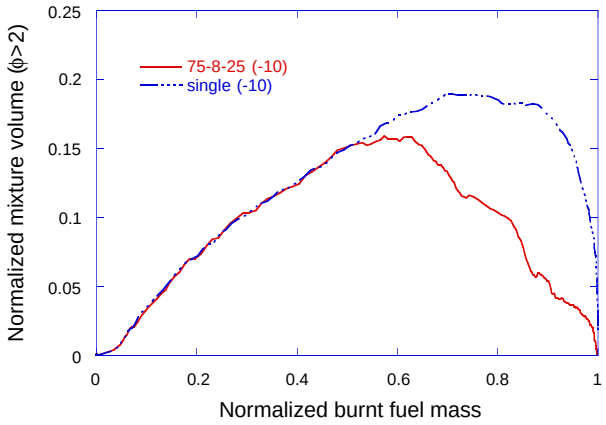

Figure 19 In-cylinder rich mixture volume normalized by the instantaneous total volume showing the effects of the second-pulse injection on fuel/air mixing.

SOOT REDUCTION MECHANISM - As indicated in Fig. 13, some multiple injection schemes can reduce soot emissions significantly, while some can increase soot emissions. Figure 17 gives the soot production history during the combustion process for the various cases. It is seen that the in-cylinder soot production histories of the multiple injections are changed significantly from the original single injection cases. The peak values of in-cylinder soot from the multiple injections are largely reduced due to the injection pause, and the net productions have different values at the end of combustion. It is known that the net soot production is the result of the competition between soot formation and soot oxidation. This is illustrated in Fig. 18 in which the 75-8-25 (-10) and single (-10) cases are compared. It is seen that the injection pause affects both the soot formation and oxidation processes and depresses the soot chemistry. However, the soot formation is reduced more than the soot oxidation (as indicated by the numbers and arrows in the figure). Therefore, the formation-oxidation competition results in a significant reduction of soot production in the 75-8-25 (-10) case (factor of 4). It is expected that the second-pulse injected spray also

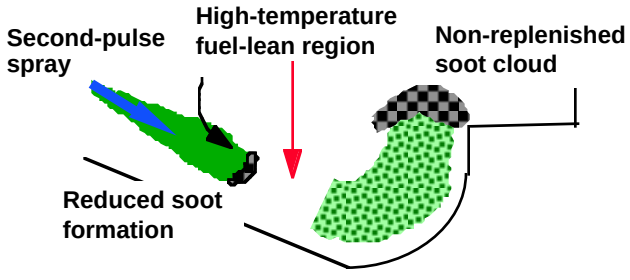

Figure 20 Schematic diagram showing soot-reduction mechanisms of split injections. Left: Single injection. Right: Split injection.

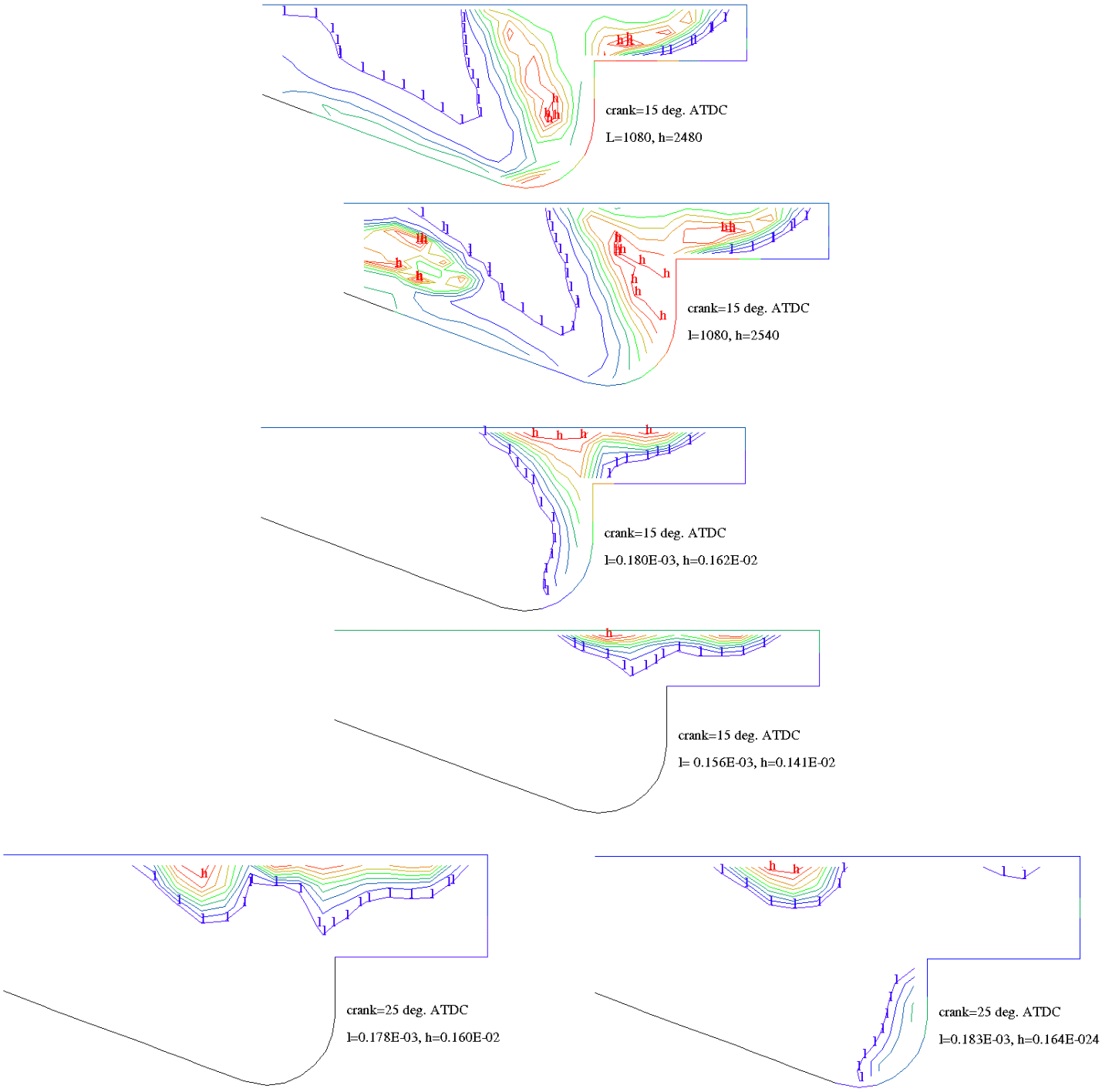

Figure 21 Computed temperature (K) (top) and soot concentration (g/cm^3) (middle and bottom) contours in the plane of the spray axis. Left: Single injection (-10). Right: Split injection 75-8-25 (-10).

enhances fuel-air mixing. This reasoning is supported by Fig. 19 which shows the change of the in-cylinder gas volume containing rich mixtures (equivalence ratio greater than 2.0) as function of the burnt fuel mass. As can be seen, the amount of rich mixture is reduced significantly after the injection pause in the 75-8-25 (-10) double injection case because of the dispersion of the fuel/air mixture between the injection pulses which is no longer maintained by the high momentum fuel jet. This process tends to lean out the mixture. Soot formation is therefore reduced.

The mechanisms of for the soot reduction using split injections are illustrated schematically in Fig. 20. Soot is formed and accumulates in the tip region of the spray jet. This soot accumulation at the spray tip has also been observed experimentally by Dec and Espey in an optically accessible DI diesel engine [26]. In single injection combustion, the high momentum injected fuel penetrates to the fuel-rich, relatively

low temperature region at the jet tip and continuously replenishes the rich region, producing soot. In a split-injection, however, the second-pulse injected fuel enters into a relatively fuel-lean and high-temperature region which is left over from the combustion of the first pulse. Soot formation is therefore significantly reduced because the injected fuel is rapidly consumed by combustion before a rich soot-producing region can accumulate. This can also be seen in Fig. 19, where the last 25% of the injection is seen not to increase the amount of rich mixture in the chamber. In addition, the soot cloud of the first spray plume is not replenished with fresh fuel, instead, continues to oxidize. As a result, the net production of soot in split-injection combustion can be reduced substantially, particularly if the dwell between the two injections is optimized – long enough that the soot formation region of the first injection is not replenished with fresh fuel, but short enough that the in-cylinder gas temperature environment seen by the second pulse remains high enough to prompt fast combustion, reducing soot formation.

This mechanism is demonstrated in the computed results shown in Fig. 21. Although the computed soot distributions are complicated by the gas flow motion and wall/spray interactions, it is seen clearly that the high soot region is located in the leading portion of the spray-induced flow in both the single and split injection cases (see the middle row of Fig. 21 at 15 deg. ATDC). By this time the leading edge of the first formed soot cloud has moved up the bowl and is located on the cylinder head. In the single injection case, the larger quantity of soot formed is being oxidized (a larger quantity because this region was replenished with fresh fuel until the end of the injection). As a result, the amount of total in-cylinder soot is reduced by 25 deg. ATDC (left-bottom plot in Fig. 21, also see Fig. 18). However, in the split injection case, the second-pulse injected fuel forms a separate burning region near the nozzle at 15 deg. ATDC, as seen in the temperature contours of the right-top plot. The fuel-air mixture becomes relatively lean compared with the single injection case as was shown in Fig. 19. Since the soot formation of the second spray plume is greatly reduced, no appreciable soot is produced in this region at this time. By 25 deg. ATDC, however, some amount of soot is seen to have been produced from the second spray plume deep in the bowl, but its concentration is very low relative to that from the first spray plume.

The above results explain why multiple injections can improve the soot-NOx trade-off. On the other hand, soot increased for the 25-8-75 (-10) case. As discussed before, the major portion of the combustion process in the 25-8-75 (-10) case is delayed by the injection pause, thus it is expected that the soot production mechanism in this case is similar to that of a single injection case with retarded injection timing in which soot emissions increase due to the deteriorated soot oxidation. This is indeed seen by comparing the 25-8-75 (-10) case with the single (-2) case in Fig. 17.

It is expected that further emissions reductions could be obtained if the injection timing was also varied. For example, the predicted soot-NO trade-off trend using different injection schemes is illustrated in Fig. 22. It is clearly seen that the 75-8-25 double injection shifts the soot-NO trade-off to a lower level of soot emission relative to that of the single injection with almost no penalty in the NO emission in the timing range studied (from -14 to +2 ATDC) when the same

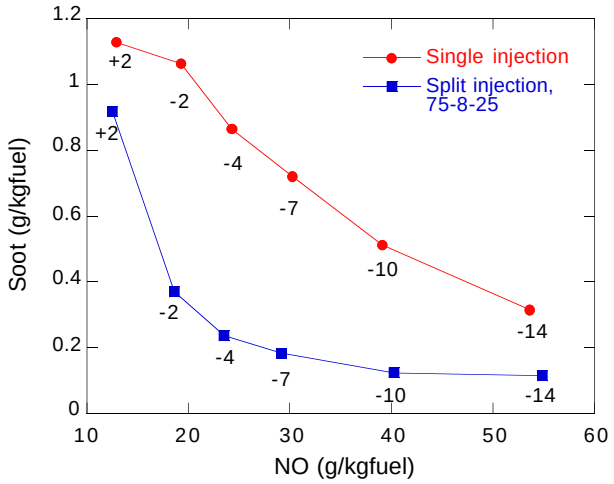

Figure 22 Computed soot-NO trade-off showing predicted emission reduction using split injections. Numbers in the figure are the injection timings (ATDC).

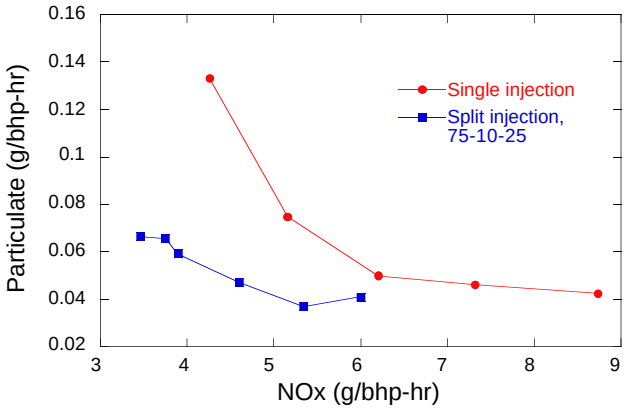

Figure 23 Measured particulate-NOx trade-off of a Caterpillar engine at 75% load for single and double injections [3]. Injection timings were varied from -12 to +1 ATDC.

injection timing is used for the two injection schemes. In the single injection cases, NO can be reduced with a corresponding penalty of increased soot with retarding injection timings. This phenomenon is also seen in the 75-8-25 split injection case. However, with the combination of double injections and retarded injection timings, significant reductions of NO and soot can be achieved simultaneously. These predicted resultsare consistent with the experimental observations of Tow et al. [3] shown in Fig. 23 which demonstrates the dramatic reduction of

particulate that has been observed with a 75-10-25 double injection. It is worth noting that even larger emission reductions have been observed using triple and quadruple injection in combustion with EGR [6].

SUMMARY AND CONCLUSIONS

Computations were made of diesel engine combustion with multiple fuel injections. Improved multiple-injection combustion predictions were obtained using a RNG k-ε turbulence model, a new wall heat transfer model and the nozzle discharge coefficient in the injection model to simulate the contraction of fuel jet at the nozzle exit.

It was found that the turbulence model and the nozzle discharge coefficient affect combustion modeling significantly. The original KIVA heat transfer model cannot predict the heat transfer direction change during the compression stroke and greatly underpredicts wall heat flux during combustion. Although the wall heat transfer calculation seems not to affect heat release prediction significantly, it does affect the computed cylinder pressure due to energy conservation.

The present model was validated by comparisons with different measured multiple injection schemes. The computed cylinder pressure, heat release rate and soot and NOx emissions were compared with measured data. Good agreement was obtained in most cases. However, some disagreement was found in the premixed-burn phase for the cases with 10% fuel injected in the first injection pulse. This indicates more model improvement may be necessary.

The computations show that a split injection with a small percentage (e.g., 25%) of fuel in the second injection pulse can significantly reduce soot production while not increasing NO formation levels appreciably. It is confirmed by the computations that soot emission can be reduced by using split injections, and, split injection also allows the injection timing to be retarded to reduce NOx emission. By using a split injection scheme with retarded injection timings, both soot and NOx can be reduced simultaneously. These findings reproduce experimental results which show the benefit of using multiple injections [2-6].

The mechanism of soot and NO reduction using multiple injections was studied computationally using a designed set of model injection schemes. Based on the computational results, the NO reduction mechanism is found to be similar to that of a single injection with retarded injection timing. Regarding soot reduction, soot formation is reduced after the injection pause between injection pulses. The reduced soot formation is shown to be due to the fact that the soot producing rich regions at the spray tip are no longer replenished. During the dwell between injection pulses, the mixture becomes leaner. With multiple injections, multiple soot formation regions are formed in the combustion chamber, but, since the subsequent injections take place into a high temperature environment left from the combustion products of the first injection, the injected fuel burns more rapidly, soot formation rates are decreased, and the net soot production can be reduced dramatically.

Interestingly, it is also found that a single injection with a longer injection duration gives similar emission reduction results to that of a 50-8-50 double injection which has a similar combustion history. However, the single injection requires the use of smaller nozzle hole sizes for the same injected quantity. The use of multiple injections hence gives greatly increased flexibility in designing injection schemes for emissions reduction.

ACKNOWLEDGMENTS

This work was supported by Ford Motor Co., Caterpillar Engine Co., DOE/NASA-Lewis and the Army Research Office. Support for the computations was provided by Tacom, San Diego Supercomputer Center and by Cray Research, Inc. The helpful comments of Prof. Chris Rutland are appreciated. The authors also thank Mike Chan for providing additional data in Fig. 22.

REFERENCES

1. Pierpont, D. A. and Reitz, R. D., “Effects of Injection Pressure and Nozzle Geometry on Emissions and Performance in a D.I Diesel,” SAE Paper 950604, 1995.

2. Nehmer, D. A. and Reitz, R. D., "Measurement of the Effect of Injection Rate and Split Injections on Diesel Engine Soot and NOx Emissions," SAE Paper 940668, 1994.

3. Tow, T., Pierpont, A. and Reitz, R. D., "Reducing Particulates and NOx Emissions by Using Multiple Injections in a Heavy Duty D.I. Diesel Engine," SAE Paper 940897, 1994.

4. Pierpont, D. A., Montgomery, D. T. and Reitz, R. D., “Reducing Particulate and NOx Using Multiple Injections and EGR in a D. I. Diesel,” SAE Paper 950217, 1995.

5. Shundoh, S., Komori, M., Tsujimur, K. and Kobayashi, S., “NOx Reduction from Diesel Combustion Using Pilot Injection with High Pressure Fuel Injection,” SAE Paper 920461, 1992.

6. Montgomery, D. T., and Reitz, R. D., “Six-mode Cycle Evaluation of the Effect of EGR and Multiple Injections on Particulate and NOx Emissions from a D. I. Diesel Engine,” SAE Paper 960316, 1996.

7. Patterson, M. A., Kong, S. -C., Hampson, G. J. and Reitz, R. D., "Modeling the Effects of Fuel Injection Characteristics on Diesel Engine Soot and NOx Emissions," SAE Paper 940523, 1994.

8. Kong, S. -C., Han, Z., and Reitz, R. D., “The Development and Application of a Diesel Ignition and Combustion Model for Multidimensional Engine Simulation,” SAE Paper 950278, 1995.

9. Han, Z., and Reitz, R. D., “Turbulence Modeling of Internal Combustion Engines Using RNG k-ε models”, *Comb. Sci. Tech.*, **106**, 4-6, 267, 1995.

10. Amsden, A. A., O'Rourke, P. J. and Butler, T. D., "KIVA-II - A Computer Program for Chemically Reactive Flows with Sprays," Los Alamos National Labs., LA-11560- MS, 1989.

11. Yakhot, V., and Orszag, S. A. “Renormalization Group Analysis of Turbulence. I. Basic Theory.” *J. Sci. Comput*., **1**, 3, 1986.

12. Han, Z., and Reitz, R. D., “A Temperature Wall Function Formulation for Variable-Density Turbulence Flows with Application to Engine Convective Heat Transfer

Modeling," submitted to *International Journal of Heat and Mass Transfer*, 1995.

13. Kays, W. M., and Crawfold, M. E., *Convective Heat and Mass Transfer*, McGraw-Hill Company, 1980.

14. Reitz, R. D., "Modeling Atomization Processes in High-Pressure Vaporizing Sprays. *Atomization and Spray Technology*, " **3**, 309, 1987.

15. Chaves, H., Knapp, M., Kubitzek, A., Obermeier, F., and Schneider, T., " Experimental Study of Cavitation in the Nozzle Hole of Diesel Injectors Using Transparent Nozzles," SAE Paper 950290, 1995.

16. Bowman, C. T. "Kinetics of Pollutant Formation and Destruction in Combustion," *Prog. Energy Combust. Sci.*, **1**, 33, 1975.

17. Heywood, J. B., *Internal Combustion Engine Fundamentals*, McGraw-Hill Company, 1988.

18. Hampson, G. J., Lui, Y., Han, Z., and Reitz, R. D., "Modeling of NOx Emissions with Comparison to Exhaust Measurements for a Gas Fuel Converted Heavy-Duty Diesel Engine," in preparation.

19. Hiroyasu, H. and Kadota, T., "Models foe Combustion and Formation of Nitric Oxide and Soot in DI Diesel Engines," SAE Paper 760129, 1976.

20. Belarduni, P., Bertoli, C., Ciajolo, A., D'Anna, A. and Del Giacomo, N., "Three-Dimensional Calculations with In Cylinder Sampling Valve Data," SAE Paper 922225, 1992.

21. Nagle, J. Strickland-Constable, R. F., "Oxidation of Carbon between 1000-2000 C," Proc. of the Fifth Carbon Conf., Volume 1, Pergammon Press, p. 154, 1962.

22. Hampson, G. J. and Reitz, R. D., "Development of NOx and Soot Models for Multidimensional Diesel Combustion," accepted by the ASME International Joint Power Generation Conference, Minneapolis, MN, 1995.

23. Reitz, R. D., "Assessment of Wall Heat Transfer Models for Premixed-Charge Engine Combustion Computations," SAE Paper 910267, 1991.

24. Tow, C. T., "The Effect of Multiple Pules Injection, Injection Rate and Injection Pressure on Particulate and NOx Emissions from a D.I. Diesel Engine," Master thesis, University of Wisconsin-Madison, 1993.
25. Ricart, L. M., and Reitz, R. D., "Visualization and Modeling of Pilot Injection and Combustion in Diesel Engines," SAE Paper 960833, 1996.

26. Dec, J. E., and Espey, C., "Ignition and Early Soot Formation in a DI Diesel Engine Using Multiple 2-D Imaging Diagnostics," SAE Paper 950456, 1995.